THE JOURNAL OF PHYSICAL CHEMISTRY C

pubs.acs.org/JPCC Article

Order–Disorder Transition in Kesterite Cu_2ZnSnS_4: Thermopower Enhancement via Electronic Band Structure Modification

Eleonora Isotta, Binayak Mukherjee, Carlo Fanciulli, Nicola M. Pugno, and Paolo Scardi*

Cite This: J. Phys. Chem. C 2020, 124, 7091–7096 Read Online

ACCESS | Metrics & More | Article Recommendations | Supporting Information

ABSTRACT: The order–disorder transition of kesterite (CZTS, Cu_2ZnSnS_4) from $I\bar{4}$ to $I\bar{4}2m$ crystal structures has a marked effect on Seebeck coefficient, which displays a sharp enhancement at the transition temperature, around 533 K. Considered to be detrimental for the performance of photovoltaic kesterite, the order–disorder transition appears to be beneficial for thermopower. Experimental data and ab initio calculations explain the origin of this enhancement: the increase of crystal symmetry in the disordered polymorph leads to a favorable electronic band structure characterized by flat and converged bands. At the transition, a sharp drop in mobility and increase in carrier concentration experimentally prove this mechanism of Seebeck enhancement. This, other than providing a new understanding of the material, can cast light on some profitable mechanisms to enhance the thermoelectric performance. Additionally, the increase in Seebeck provides an efficient tool to observe the transition and possibly to quantify disorder.

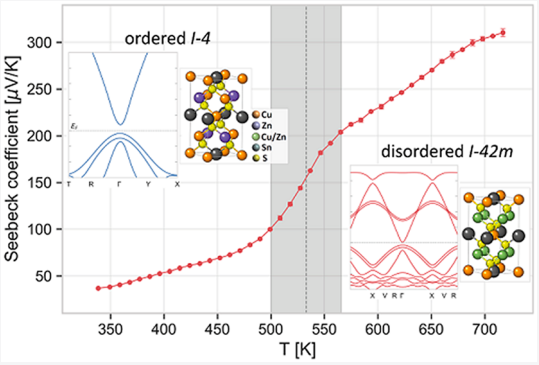

1. INTRODUCTION

Kesterite (CZTS) is a *p*-type chalcogenide material with reference formula Cu_2ZnSnS_4. It has long been studied as absorber in thin film photovoltaic devices,[1−3] and recently deemed promising as a potential thermoelectric material,[4−10] valued for its intrinsically low thermal conductivity[4] and composition based on nontoxic, abundant and low-cost elements.[11] In its ordered and low temperature form, kesterite is reported having a tetragonal $I\bar{4}$ crystal structure, while it was recently proved that a cubic $F\bar{4}3m$ low-temperature polymorph can be obtained for samples made by high-energy ball-milling, as an effect of a high disorder state of the cations.[4,12] This appears to be a metastable phase, since it transitions to the tetragonal polymorph on heating, as the temperature activates a reordering of the cations.[4] At around 533 K, tetragonal kesterite faces a reversible order–disorder phase transition: cations in the intermediate Cu–Zn planes of the $I\bar{4}$ structure (*2c* and *2d* Wyckoff positions) completely randomize their position (becoming *4d* Wyckoff position) thus transitioning to the tetragonal $I\bar{4}2m$ structure.[5,13−15] This transition has been studied in some detail in recent years, because disorder is considered detrimental for the photovoltaic performance of CZTS, as well as difficult to avoid. In fact, owing to the low formation energy of the Cu_{Zn} and Zn_{Cu} antisite defects,[16,17] a certain degree of disorder is inevitable in CZTS, even after extensive annealing treatments. Significant efforts have been made to quantify the degree of disorder and the subsequent loss in photovoltaic efficiency, rarely finding an ultimately suitable technique.[5,14] Nevertheless, for what concerns thermoelectric performance things proved to be different: the order–disorder transition has a marked and beneficial effect on the Seebeck coefficient.[5]

The aim of this work is to demonstrate experimentally and through ab initio calculations the physical origin of the increase in thermopower caused by the order–disorder transition of kesterite, which we connect with the crystal-symmetry induced modification of the electronic band structure. We also show how the degree of order of a sample affects the Seebeck coefficient.

2. METHODS

2.1. Experimental Section. Bulk kesterite sintered disks were produced according to previously described procedures,[4,5] starting from reactive ball milling of the elementary components, that is, metals and sulfur in stoichiometric proportions, to obtain kesterite nanometric powders, then cold-pressed and thermally treated. Some of the samples undergone a quenching process in air, either starting from the sintering temperature of 560 °C, or from a lower temperature reached with natural cooling, to room temperature. Absolute

Received: January 31, 2020
Revised: March 5, 2020
Published: March 9, 2020

https://dx.doi.org/10.1021/acs.jpcc.0c00886
J. Phys. Chem. C 2020, 124, 7091–7096

Seebeck coefficient measurements have been performed in 4-contact configuration and with Pt standard with a Linseis LZT Meter, in the temperature range 320−720 K, with a temperature gradient of 10K. Carrier density and mobility have been measured with an MMR K-20 and an H-50 measurement systems. Results are obtained by a combined measurement of Hall effect and resistivity as a function of temperature. Resistivity is determined by the Van Der Pauw method using squared shaped samples with thickness below 1 mm, providing an optimal geometrical ratio between surface and thickness. Hall effect measurements have been performed with a permanent-magnet field of 6270 ± 10 G. The currents for testing have been set to values below 10 mA in order to prevent any thermal change in the samples. All the measurements are performed in vacuum, to prevent material degradation, and in the temperature range 300−620 K.

2.2. Density Functional Theory (DFT) Calculations. The ab initio electronic structure calculations with DFT have been performed using the plane wave basis set implemented in the Vienna ab initio simulation package (VASP).[18,19] The electron-exchange correlation functional was approximated using the Perdew−Burke−Ernzerhof (PBE)[20] form of the generalized gradient approximation (GGA). All calculations were performed with an energy cutoff of 300 eV. The ordered and disordered structures were modeled with 16 and 64 atom supercells respectively, visible in Figure 1, and the geometry

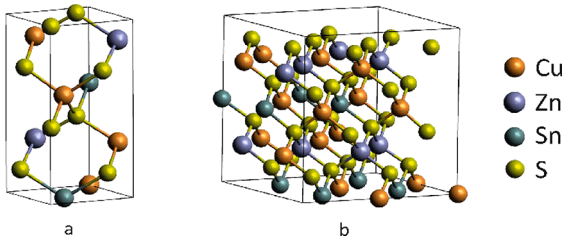

Figure 1. Supercell crystal structures of kesterite used in DFT calculations: (a) ordered, s.g. $I\bar{4}$ and 16-atom cell; (b) disordered, s.g. $I\bar{4}2m$ and 64-atom supercell.

was optimized with an 8 × 8 × 8 and 4 × 4 × 4 Monkhorst Pack (MP) k-mesh, respectively, centered at the Γ point, with Gaussian charge smearing in the order of 0.01 eV. The electronic degrees of freedom were relaxed until the change in the total free energy and energy eigenvalues were both smaller than 10^{-6} eV. The disordered structure was generated by manually assigning a random Cu/Zn arrangement in the *4d* Wyckoff positions of the $I\bar{4}2m$ structure, keeping the overall stoichiometry balanced (Cu:Zn = 1:1 in *4d* sites). The bands were calculated along a high-symmetry path in the irreducible Brillouin zone obtained using the SeeK-path[21] tool, while the electronic density of states (DoS) was obtained using a dense 24 × 24 × 24 MP k-mesh for the 16-atom supercell and an 8 × 8 × 8 MP k-mesh for the 64-atom supercells.

3. RESULTS AND DISCUSSION

3.1. Thermoelectric Properties. The order−disorder phase transition of kesterite, from the ordered $I\bar{4}$ to the disordered $I\bar{4}2m$ tetragonal structures, has been reported at 533 ± 10 K.[13,14] As shown by thermal analyses, it is a second-order and reversible transition,[5] and it consists of a full occupational disorder of Cu and Zn cations in the *4d* Wyckoff positions. This transition appears to have a beneficial role for thermoelectric CZTS. Indeed, the measurement of Seebeck coefficient, reproduced in Figure 2a, displays a sharp increase around the transition temperature.[5] Insets of Figure 2a show the ordered $I\bar{4}$ crystal structure for the region below the transition temperature, where Cu and Zn occupy specific positions in the intermediate planes, and the disordered $I\bar{4}2m$ structure for the high-temperature region, where a unique position is considered to account for a mixed and random occupation of the two cations. We have put forward that this enhancement is due to a higher symmetry in the crystal structure of disordered CZTS.[5] Indeed, due to this loss of specificity in the positions of Cu and Zn, the disordered is a more symmetric structure. This can also be noticed by the additional 2-fold rotation axis and mirror plane specified in the space group $I\bar{4}2m$.

Figure 2b shows the electrical resistivity measured in Van Der Pauw configuration, while Figure 2c displays the carrier concentration, measured via Hall effect on the same sample, and the carrier mobility, calculated from resistivity and carrier concentration data. Around the order−disorder transition temperature, we notice a substantial increase in carrier concentration, that nearly triples its values and a corresponding decrease in mobility. We observe a kink in resistivity (Figure 2b) around the transition temperature. It is worth mentioning that literature data reports a smaller electronic bandgap *Eg* for disordered kesterite (∼1.50 eV) with respect to ordered (∼1.67 eV).[15,22]

3.2. Electronic Band Structure. In order to provide a theoretical explanation for the experimentally observed changes in thermopower, electrical resistivity, carrier mobility and carrier concentration caused by the order−disorder transition, we performed ab initio band structure calculations for ordered (Figure 3a) and disordered (Figure 3b) kesterite. From these calculations we observe a 3-fold effect on the bands caused by the transition from the ordered to the disordered phase. First, we see an increased convergence at the top of the valence band in the disordered phase, with the separation between the top three bands dropping from 0.139 eV (∼5.51 kT, calculated at T = 298 K) for the ordered phase to 0.072 eV (∼1.39 kT, calculated at T = 600 K) for the disordered. Second, we observe a significant reduction in curvature (flattening) at the top of the valence band in the disordered phase compared to the ordered. Finally, we observe a decrease in the band gap going from the ordered to the disordered phase, though it must be considered that the exchange-correlation functional in GGA is known to strongly underestimate the band gap. While more sophisticated calculations using hybrid functionals do provide a better estimation of the band gap, they become prohibitively expensive in terms of computational resources, particularly for larger supercells such as the disordered structures. It may be assumed that the errors for similar systems are similar and cancel out in comparative studies, the accuracy of the calculations being validated by their agreement with experiments. The effect of an increased band convergence and a reduced curvature due to higher disorder in the crystal structure is evidenced also by the density of states (DoS), presented in Figure 3c, which is higher at the top of the valence band, with steeper slope of DoS (and of ln(DoS), in the inset) for the disordered phase with respect to the ordered. The asymmetry of the DoS with respect to the Fermi level is consistent with the *p* character of the material. In the Supporting Information, the extended band structures are visible, as well as the band structures for a partially disordered

https://dx.doi.org/10.1021/acs.jpcc.0c00886
J. Phys. Chem. C 2020, 124, 7091−7096

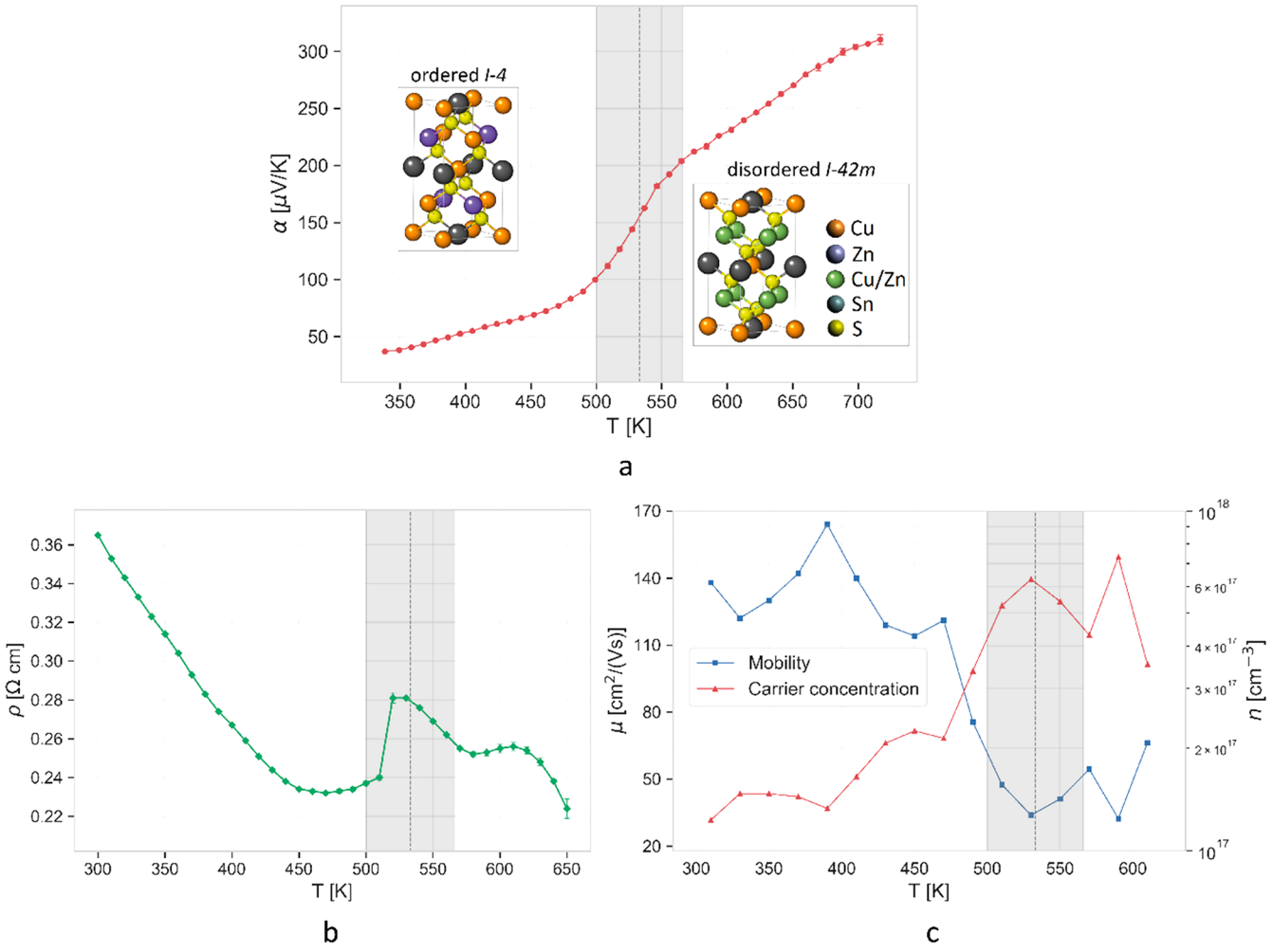

Figure 2. (a) Absolute Seebeck coefficient α (standard deviation is expressed with error bars) with insets showing the relevant kesterite crystal structures for each temperature region, namely, ordered $I\bar{4}$ in the low-temperature and disordered $I\bar{4}2m$ in the high-temperature zone. Data reproduced with permission from ref 5. Copyright 2019 MDPI. (b) Electrical resistivity ρ (standard deviation is expressed with error bars), and (c) carrier mobility μ and concentration n (in logarithmic scale) measured for a bulk CZTS sample. In the order−disorder transition region (highlighted in gray) it is possible to notice an increase in Seebeck coefficient and carrier concentration, and a corresponding drop in the mobility. This is attributed to band structure modifications: crystal-symmetry induced band convergence and reduction of curvature.

sample and another configuration of disorder, to confirm and generalize the validity of the DFT results.

3.3. Order−Disorder Transition: Crystal Symmetry Induces Band Convergence and Flatness. The thermopower is directly proportional to the density of state effective mass $m^*_{DoS} = N_V^{2/3} m_I^*$, where N_V is the band degeneracy and m_I^* is the inertial effective mass of charge carriers along the conduction direction.[23] It has been pointed out in the literature that there may be a connection between an increase in the symmetry of a crystal structure and an improved band convergence.[24−26] We believe the order−disorder transition of CZTS to be an example of this behavior: the higher crystal symmetry causes an increase in the electronic band degeneracy N_V, as proved by DFT, thus justifying the sharp growth in the experimentally observed Seebeck coefficient. We attribute the observed increase in carrier concentration (Figure 2b) both to the decrease in *Eg* and to the convergence of bands. In fact, were it due to a narrower bandgap alone, we would expect a corresponding decrease in thermopower and electrical resistivity, while experimental data shows that thermopower increases with the transition whereas resistivity does not decrease. A higher band convergence could instead explain why we observe an enhancement of Seebeck despite the increase in carrier concentration. Resistivity displays a sharp upward kink around the transition temperature and then smoothly decreases to reach values in the order of those obtained prior to the transition. This is also in contradiction with the increased carrier concentration and can only be explained with the observed sharp drop in mobility, which in this case we associate to a carrier localization due to band convergence. In many literature cases, a pronounced decrease in mobility is associated with an enhancement of thermopower,[27] along with a steeper DoS, as expressed by Mott's formula.[28] Moreover, from ab initio calculations, we observe a reduced curvature in the valence bands, which is in agreement with an increased m_I^* and decreased mobility. Indeed, the movement of cations and the concurring rearrangement of covalent bonds happening during the transition might have promoted a higher number of available energy levels (therefore, higher carrier concentration) but more localized (causing the drop in mobility and the increase in Seebeck coefficient). This, contrary to what is reported for other systems[29,30] seems to not extensively penalize electrical resistivity owing to the simultaneous increase in carrier

https://dx.doi.org/10.1021/acs.jpcc.0c00886
J. Phys. Chem. C 2020, 124, 7091−7096

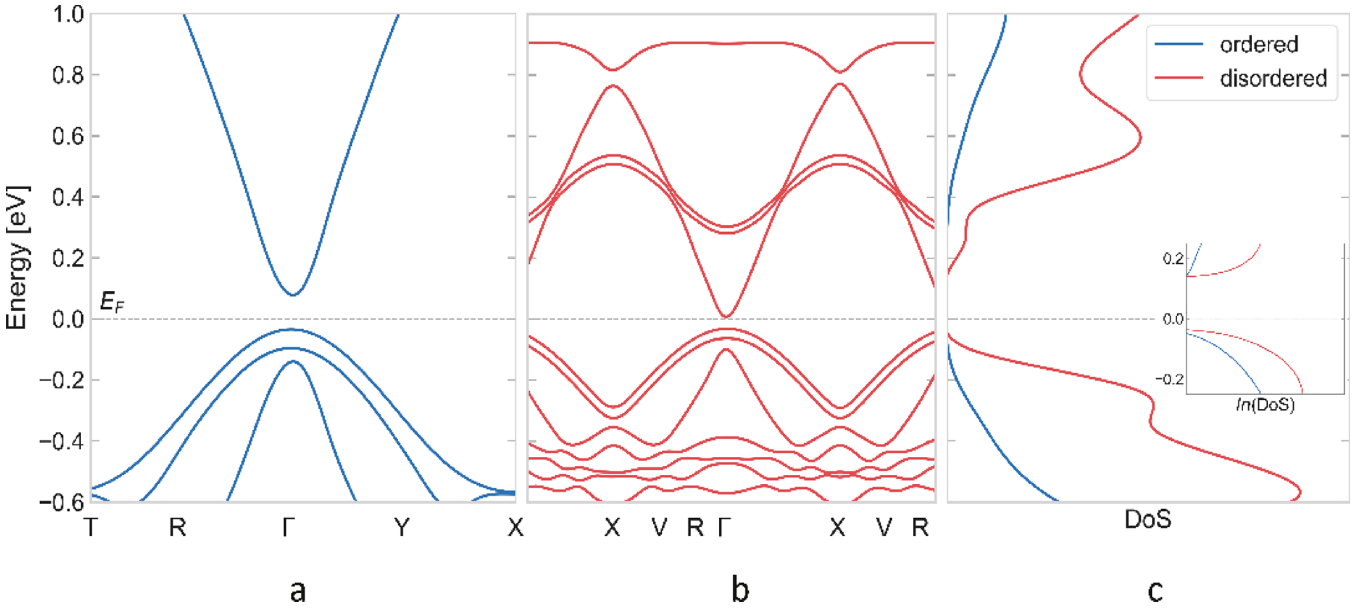

Figure 3. Band structures for ordered (a), and disordered (b) kesterite. Panel (c) displays the density of states DoS, with inset showing the natural logarithm of the DoS. With an increase of disorder, the top valence bands tend to converge and reduce their curvature, the bandgap narrows, while DoS and ln(DoS) get higher and steeper. We believe this band structure modification is at the origin of the transition. The Fermi energy is set to 0 eV in each case. *X*-axis is on the same scale in *k*-space for (a) and (b).

concentration caused by band convergence. The DoS, being higher for the disordered phase, highlights the higher availability of valence states close to the Fermi level and their higher occupation, associated with the reduced bandgap. The trend of the logarithm of the density of states (shown in the inset of Figure 3c) is steeper at the top of the valence band for the disordered polymorph, in agreement with the higher thermopower provided for by Mott's formula.[28] Furthermore, a sharper asymmetry of the DoS with respect to the Fermi level is found, which is consistent with the *p*-type nature and is typically associated with an increase in Seebeck coefficient.[28] In general, the DFT calculations are in good agreement with the experimental results. It is evident that the described phenomenon is dominated by band features (flatness and degeneracy), which is also supported by the low value of carrier concentration (in the order of 10^{17} cm^{-3}) and can explain why we observe a decoupling of the thermopower and resistivity trends. These results provide experimental and theoretical proof that favorable band structure and the subsequent enhancement of thermoelectric properties can be achieved with an increase in crystal symmetry.

3.4. Seebeck as a Method To Observe the Transition and Estimate the Degree of Order. In the photovoltaic community, much research has been performed on methods to determine the degree of order in kesterite samples, as the lower bandgap of the disordered phase is deemed responsible for open-circuit voltage losses, thus, undermining the solar-cell efficiency.[13] However, the search for a suitable and convenient technique, able to observe a clear difference between samples with different degrees of order, has proved a complex challenge. In fact, X-ray diffraction is not suitable for observing Cu−Zn disorder, because Cu^+ and Zn^{2+} are isoelectronic and appear identical to X-rays. Other proposed methods include Raman spectroscopy, through the quantification of the relative intensity of secondary peaks,[13,14,31,32] optical measurements,[15,22] solid-state nuclear magnetic resonance,[33] and neutron scattering.[34] In this context, we tentatively propose the Seebeck measurement as an alternative technique, as it proves efficient in observing the Cu−Zn transition of kesterite and sensitive to the degree of order in the sample. Indeed, we have experimentally observed that according to the level of order in the crystal structure at the beginning of the measurement, the transition appears in a different way. Figure 4 shows the trends of Seebeck coefficient for some of our

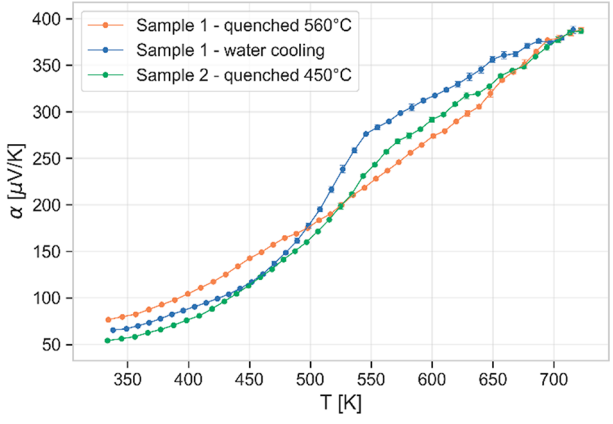

Figure 4. Absolute Seebeck coefficient α for some CZTS samples: quenched from 560 °C to preserve the disordered state, for the same sample after water cooling, and for a second sample, characterized by an intermediate disorder state.

CZTS samples characterized by different thermal histories, which is known to influence the degree of order.[13,14] Sample 1 has been obtained by quenching right after the sintering process, at 560 °C. This has been done to quench the fully disordered state of the crystal structure, and indeed the sample, on following heating, exhibits a flat trend of Seebeck coefficient, proving that no transition occurs.[5] A second measurement was then performed on the same sample after letting it to slowly cool down to ambient temperature (water

https://dx.doi.org/10.1021/acs.jpcc.0c00886
J. Phys. Chem. C 2020, 124, 7091−7096

cooling, ∼2 h long). Sample 2 has instead been obtained by allowing it to naturally cool down to 450 °C after the thermal treatment and then suddenly quenched to room temperature. The measurement of Seebeck coefficient displays a small increase around the transition temperature, pointing out that the sample was in a partially disordered state. These measurements point out that the degree of order can influence the behavior of Seebeck coefficient. Several research groups working on thermoelectric CZTS have reported different trends for the Seebeck coefficient: some of them present a flat curve that apparently does not display the order−disorder transition;[6,7] Sharma et al., instead, report trends where an increase is visible around the transition temperature.[9,10] Based on the present results, the reason for this inconsistency of experimental results can be ascribed to different degrees of order, as samples from the literature have diverse production routes and thermal histories, therefore being different in terms of ordering kinetics. Moreover, the band structure for a partially disordered sample, shown in Figure S3a of the Supporting Information, exhibits an intermediate behavior with respect to the ordered and fully disordered one, with a closer similarity to the latter. This is consistent with the definition of random occupation of Cu and Zn cations for the disordered structure, which will also include some narrow regions of order.

Nevertheless, this dependence could be exploited to retrieve information on the sample, here just qualitatively illustrated. Through a suitable empirical calibration with other techniques or a suitable theoretical model, thermopower could be used to retrieve an order parameter and to estimate the degree of order in a sample.

4. CONCLUSIONS

The order−disorder transition of kesterite from ordered $I\bar{4}$ to disordered $I\bar{4}2m$ crystal structures leads to a beneficial effect on thermopower that presents an increase around the transition temperature of 533 K,[5] conversely to what happens for photovoltaic kesterite for which the transition is deemed detrimental for the performance.[14] In this work, we have demonstrated that the mechanism at the origin of this enhancement of Seebeck coefficient is an improved electronic band structure. DFT calculations show more converged and flatter bands for the disordered polymorph, which lead to an increased carrier concentration and a decreased mobility, confirmed by experimental data. A higher crystal symmetry for the disordered structure is deemed responsible for the improved band degeneracy, which in turn leads to a higher density of states effective mass and enhanced thermopower. Electrical resistivity, differently from what commonly occurs,[29,30] is not penalized by the low mobility due to the concurrent high carrier concentration originated from band convergence. These results, besides providing a new understanding of the studied material, can cast light on some profitable mechanisms to enhance the thermoelectric performance. Additionally, the measurement of Seebeck coefficient proved to be a simple and efficient way to observe the order−disorder transition of kesterite; as shown in this work, a different degree of order in the crystal structure causes the increase of Seebeck coefficient at the order−disorder transition to vary. This dependence could be exploited to estimate the degree of order in a sample, which has always been considered difficult to attribute due to the low sensitivity of other proposed methods.[13,33] Furthermore, it could explain the difference found in the literature for CZTS in the trends of Seebeck coefficient, especially where the order−disorder transition is not explicitly observed or identified.[6,7,9,10]

■ ASSOCIATED CONTENT

Supporting Information

The Supporting Information is available free of charge at https://pubs.acs.org/doi/10.1021/acs.jpcc.0c00886.

Additional DFT calculations for other configurations of disordered kesterite (PDF)

■ AUTHOR INFORMATION

Corresponding Author

Paolo Scardi − *Department of Civil, Environmental and Mechanical Engineering, University of Trento, 38123 Trento, Italy*; Phone: +39 0461 282417; Email: paolo.scardi@unitn.it

Authors

Eleonora Isotta − *Department of Civil, Environmental and Mechanical Engineering and Laboratory of Bio-inspired, Bionic, Nano, Meta Materials and Mechanics, Department of Civil, Environmental and Mechanical Engineering, University of Trento, 38123 Trento, Italy*; orcid.org/0000-0002-5864-463X

Binayak Mukherjee − *Department of Civil, Environmental and Mechanical Engineering, University of Trento, 38123 Trento, Italy*

Carlo Fanciulli − *National Research Council of Italy-Institute of Condensed Matter Chemistry and Technologies for Energy (CNR-ICMATE), 23900 Lecco, Italy*

Nicola M. Pugno − *Department of Civil, Environmental and Mechanical Engineering and Laboratory of Bio-inspired, Bionic, Nano, Meta Materials and Mechanics, Department of Civil, Environmental and Mechanical Engineering, University of Trento, 38123 Trento, Italy; Ket-Lab, Edoardo Amaldi Foundation, 00133 Rome, Italy; School of Engineering and Materials Science, Queen Mary University of London, London E1 4NS, United Kingdom*; orcid.org/0000-0003-2136-2396

Complete contact information is available at: https://pubs.acs.org/10.1021/acs.jpcc.0c00886

Author Contributions

The manuscript was written through contributions of all authors. All authors have given approval to the final version of the manuscript.

Notes

The authors declare no competing financial interest.

■ ACKNOWLEDGMENTS

This research was funded by the Autonomous Province of Trento, within the framework of the programmatic Energy Action 2015−2017. The computational time was provided by CINECA - Italian Supercomputing Facility, with the Project CZTS - HP10CONX70. N.M.P. is supported by the European Commission under the Graphene Flagship Core 2 Grant No. 785219 (WP14, "Composites"), the FET Proactive ("Neurofibers") Grant No. 732344, and the FET Open (Boheme) Grant No. 863179, as well as by the Italian Ministry of Education, University and Research (MIUR) under the "Departments of Excellence" Grant L. 232/2016, and the

ARS01-01384-PROSCAN and the PRIN-20177TTP3S Grants.

REFERENCES

(1) Katagiri, H.; Jimbo, K.; Yamada, S.; Kamimura, T.; Maw, W. S.; Fukano, T.; Ito, T.; Motohiro, T. Enhanced Conversion Efficiencies of Cu_2ZnSnS_4-Based Thin Film Solar Cells by Using Preferential Etching Technique. *Appl. Phys. Express* **2008**, *1* (4), 0412011−0412012.
(2) Ataollahi, N.; Malerba, C.; Ciancio, R.; Edla, R.; Scardi, P.; Cappelletto, E.; Di Maggio, R. Control of Composition and Grain Growth in Cu2ZnSnS4 Thin Films from Nanoparticle Inks. *Thin Solid Films* **2019**, *674*, 12−21.
(3) Syafiq, U.; Ataollahi, N.; Maggio, R. D.; Scardi, P. Solution-Based Synthesis and Characterization of Cu_2ZnSnS_4 (CZTS) Thin Films. *Molecules* **2019**, *24* (19), 3454.
(4) Isotta, E.; Pugno, N. M.; Scardi, P. Nanostructured Kesterite (Cu_2ZnSnS_4) for Applications in Thermoelectric Devices. *Powder Diffr.* **2019**, *34* (S1), 2−7.
(5) Isotta, E.; Fanciulli, C.; Pugno, N. M.; Scardi, P. Effect of the Order-Disorder Transition on the Seebeck Coefficient of Nanostructured Thermoelectric Cu2ZnSnS4. *Nanomaterials* **2019**, *9* (5), 762.
(6) Liu, M. L.; Huang, F. Q.; Chen, L. D.; Chen, I. W. A Wide-Band-Gap p -Type Thermoelectric Material Based on Quaternary Chalcogenides of Cu2ZnSnQ4(Q = S,Se). *Appl. Phys. Lett.* **2009**, *94* (20), 202103.
(7) Yang, H.; Jauregui, L. A.; Zhang, G.; Chen, Y. P.; Wu, Y. Non-Toxic and Abundant Copper Zinc Tin Sulfide Nanocrystals for Potential High Temperature Thermoelectric Energy Harvesting. *Nano Lett.* **2012**, *12*, 540.
(8) Kumar, S.; Ansari, M. Z.; Khare, N. Influence of Compactness and Formation of Metallic Secondary Phase on the Thermoelectric Properties of Cu2ZnSnS4 Thin Films. *Thin Solid Films* **2018**, *645*, 300−304.
(9) Sharma, S. D.; Neeleshwar, S. Thermoelectric Properties of Hot Pressed CZTS Micro Spheres Synthetized by Microwave Method. *MRS Adv.* **2018**, *3* (24), 1373−1378.
(10) Sharma, S. D.; Khasimsaheb, B.; Chen, Y. Y.; Neeleshwar, S. Enhanced Thermoelectric Performance of Cu 2 ZnSnS 4 (CZTS) by Incorporating Ag Nanoparticles. *Ceram. Int.* **2019**, *45* (2), 2060−2068.
(11) Adachi, S. *Earth-Abundant Materials for Solar Cells*; John Wiley and Sons, 2015.
(12) Kapusta, K.; Drygas, M.; Janik, J. F.; Jelen, P.; Bucko, M. M.; Olejniczak, Z. From Magnetic Cubic Pre-Kesterite to Semiconducting Tetragonal Kesterite Cu2ZnSnS4 Nanopowders via the Mechanochemically Assisted Route. *J. Alloys Compd.* **2019**, *770*, 981−988.
(13) Scragg, J. J. S.; Choubrac, L.; Lafond, A.; Ericson, T.; Platzer-Björkman, C. A Low-Temperature Order-Disorder Transition in Cu2ZnSnS4 Thin Films. *Appl. Phys. Lett.* **2014**, *104* (4), 041911.
(14) Scragg, J. J. S.; Larsen, J. K.; Kumar, M.; Persson, C.; Sendler, J.; Siebentritt, S.; Platzer Bjorkman, C. Cu−Zn Disorder and Band Gap Fluctuations in $Cu_2ZnSn(S,Se)_4$: Theoretical and Experimental Investigations. *Phys. Status Solidi B* **2016**, *253* (2), 247−254.
(15) Valentini, M.; Malerba, C.; Menchini, F.; Tedeschi, D.; Polimeni, A.; Capizzi, M.; Mittiga, A. Effect of the Order-Disorder Transition on the Optical Properties of Cu2ZnSnS4. *Appl. Phys. Lett.* **2016**, *108*, 211909.
(16) Chen, S.; Gong, X. G.; Walsh, A.; Wei, S. *Appl. Phys. Lett.* **2010**, *96*, 021902.
(17) Chen, S.; Walsh, A.; Gong, X.; Wei, S. Classification of Lattice Defects in the Kesterite Cu_2ZnSnS_4 and $Cu_2ZnSnSe_4$ Earth-Abundant Solar Cell Absorbers. *Adv. Mater.* **2013**, *25* (11), 1522−1539.
(18) Kresse, G.; Furthmüller, J. Efficient Iterative Schemes for Ab Initio Total-Energy Calculations Using a Plane-Wave Basis Set. *Phys. Rev. B: Condens. Matter Mater. Phys.* **1996**, *54* (16), 11169−11186.
(19) Kresse, G.; Furthmüller, J. Efficiency of Ab-Initio Total Energy Calculations for Metals and Semiconductors Using a Plane-Wave Basis Set. *Comput. Mater. Sci.* **1996**, *6* (1), 15−50.
(20) Perdew, J. P.; Burke, K.; Ernzerhof, M. Generalized Gradient Approximation Made Simple. *Phys. Rev. Lett.* **1996**, *77* (18), 3865−3868.
(21) Hinuma, Y.; Pizzi, G.; Kumagai, Y.; Oba, F.; Tanaka, I. Band Structure Diagram Paths Based on Crystallography. *Comput. Mater. Sci.* **2017**, *128*, 140−184.
(22) Malerba, C.; Valentini, M.; Mittiga, A. Cation Disorder in Cu2ZnSnS4 Thin Films: Effect on Solar Cell Performances. *Sol. RRL* **2017**, *1*, 1700101.
(23) Kittel, C. *Introduction to Solid State Physics*, 8th ed.; Wiley, 2005; DOI: 10.1119/1.1934457.
(24) Zeier, W. G.; Zhu, H.; Gibbs, Z. M.; Ceder, G.; Tremel, W.; Snyder, G. J. Band Convergence in the Non-Cubic Chalcopyrite Compounds Cu2MGeSe4. *J. Mater. Chem. C* **2014**, *2* (47), 10189−10194.
(25) Zeier, W. G. New Tricks for Optimizing Thermoelectric Materials. *Curr. Opin. Green Sustain. Chem.* **2017**, *4*, 23−28.
(26) Zhang, Q.; Song, Q.; Wang, X.; Sun, J.; Zhu, Q.; Dahal, K.; Lin, X.; Cao, F.; Zhou, J.; Chen, S. Deep Defect Level Engineering: A Strategy of Optimizing the Carrier Concentration for High Thermoelectric Performance. *Energy Environ. Sci.* **2018**, *11*, 933−940.
(27) Sun, P.; Wei, B.; Zhang, J.; Tomczak, J. M.; Strydom, A. M.; Søndergaard, M.; Iversen, B. B.; Steglich, F. Large Seebeck Effect by Charge-Mobility Engineering. *Nat. Commun.* **2015**, *6* (May), 1−5.
(28) Rohrman, F. A. The Theory of the Properties of Metals and Alloys (Mott, N. F.; Jones, H.). *J. Chem. Educ.* **1937**, *14*, 99.
(29) Pei, Y.; Wang, H.; Snyder, G. J. Band Engineering of Thermoelectric Materials. *Adv. Mater.* **2012**, *24* (46), 6125−6135.
(30) Pei, Y.; Lalonde, A. D.; Wang, H.; Snyder, G. J. Low Effective Mass Leading to High Thermoelectric Performance. *Energy Environ. Sci.* **2012**, *5* (7), 7963−7969.
(31) Rudisch, K.; Ren, Y.; Platzer-Bjorkman, C.; Scragg, J. Order-Disorder Transition in B-Type Cu_2ZnSnS_4 and Limitations of Ordering through Thermal Treatments. *Appl. Phys. Lett.* **2016**, *108*, 231902.
(32) Rudisch, K.; Davydova, A.; Platzer-Bjorkman, C.; Scragg, J. The Effect of Stoichiometry on Cu-Zn Ordering Kinetics in Cu_2ZnSnS_4 Thin Films. *J. Appl. Phys.* **2018**, *123* (October 2017), 161558.
(33) Paris, M.; Choubrac, L.; Lafond, A.; Guillot-Deudon, C.; Jobic, S. Solid-State NMR and Raman Spectroscopy To Address the Local Structure of Defects and the Tricky Issue of the Cu/Zn Disorder in Cu-Poor, Zn-Rich CZTS Materials. *Inorg. Chem.* **2014**, *53*, 8646−8653.
(34) Ritscher, A.; Hoelzel, M.; Lerch, M. The Order-Disorder Transition in Cu_2ZnSnS_4 − A Neutron Scattering Investigation. *J. Solid State Chem.* **2016**, *238*, 68.

https://dx.doi.org/10.1021/acs.jpcc.0c00886
J. Phys. Chem. C 2020, 124, 7091−7096

Order-Disorder Transition in Kesterite Cu_2ZnSnS_4: Thermopower Enhancement via Electronic Band Structure Modification

Eleonora Isotta,[a,b] Binayak Mukherjee,[a] Carlo Fanciulli,[c] Nicola M. Pugno,[a,b,d,e] and Paolo Scardi[a]*

[a] Department of Civil, Environmental and Mechanical Engineering, University of Trento, via Mesiano 77, 38123 Trento, Italy

[b] Laboratory of Bio-inspired, Bionic, Nano, Meta Materials & Mechanics, Department of Civil, Environmental and Mechanical Engineering, University of Trento, via Mesiano 77, 38123 Trento, Italy

[c] National Research Council of Italy-Institute of Condensed Matter Chemistry and Technologies for Energy (CNR-ICMATE), Lecco Unit, via Previati 1/E, 23900 Lecco, Italy

[d] Ket-Lab, Edoardo Amaldi Foundation, Via del Politecnico snc, 00133 Rome, Italy

[e] School of Engineering and Materials Science, Queen Mary University of London, Mile End Road, London E1 4NS, UK

1. Further DFT calculations

1.1 Full band structure for ordered and disordered kesterite

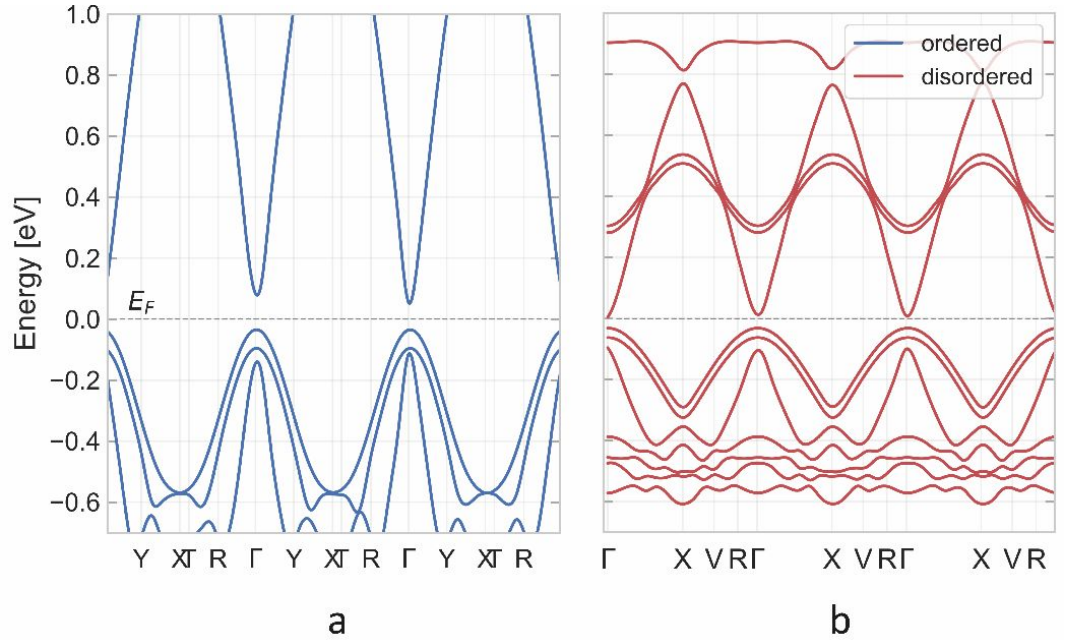

Figure S1. Full band structures for ordered (a), and disordered (b) kesterite. The reduced curvature of valence bands close to the energy gap for the disordered polymorph is clearly visible. The Fermi energy is set to 0 eV in each case. X-axis is on the same scale in k-space.

1.2 Different configurations and degrees of disorder

To allow a better understanding of the behavior of kesterite during the order-disorder transition, additional simulations were carried on with the same calculation method described in section 2.2 of the main text. A partially disordered structure was modelled by disordering half of the 64-atom supercell (Figure S2a). The relevant band structure is visible in Figure S3a, where it is possible to notice the intermediate behavior with respect to the ordered and fully disordered phase, with a closer similarity to the latter. This is consistent with the definition of random occupation of Cu and Zn cations for the disordered structure, which will also include some narrow regions of order. For what concerns the disordered structure, a 64-atom supercell cannot be representative of disorder in the real situation, which should be modelled with a computationally unfeasible much larger supercell, that accounts for additional patterns of disorder. To partially overcome this problem, we have simulated the behavior of an additional configuration of fully disordered kesterite, the supercell of which is visible in Figure S2b, and band structure in Figure S3b. The band structure shows a behavior consistent with the first simulation: although not identical, due to different cation positions and therefore a slightly different super-structure, if compared to the band structure of ordered kesterite, it is possible to observe a reduction of band gap, and flatter, more converged bands.

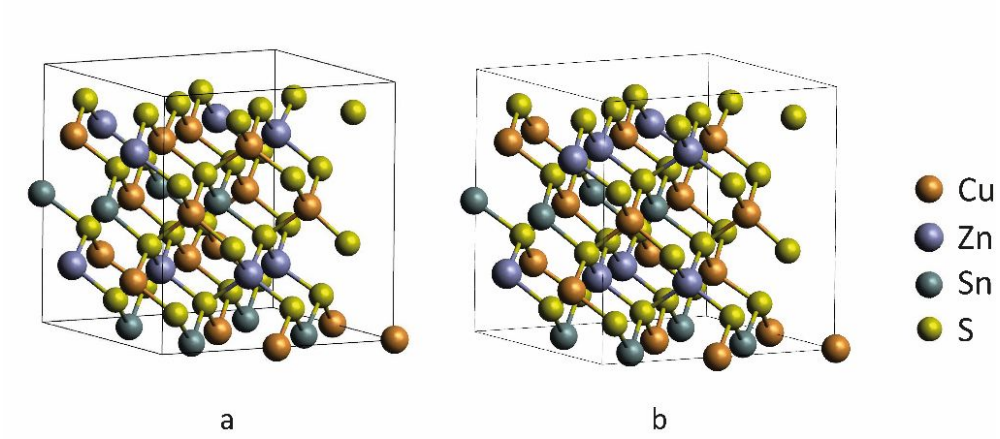

Figure S2. Supercell crystal structures of kesterite used in the additional DFT calculations simulating partial disorder, (a), and another configuration of full disorder, (b).

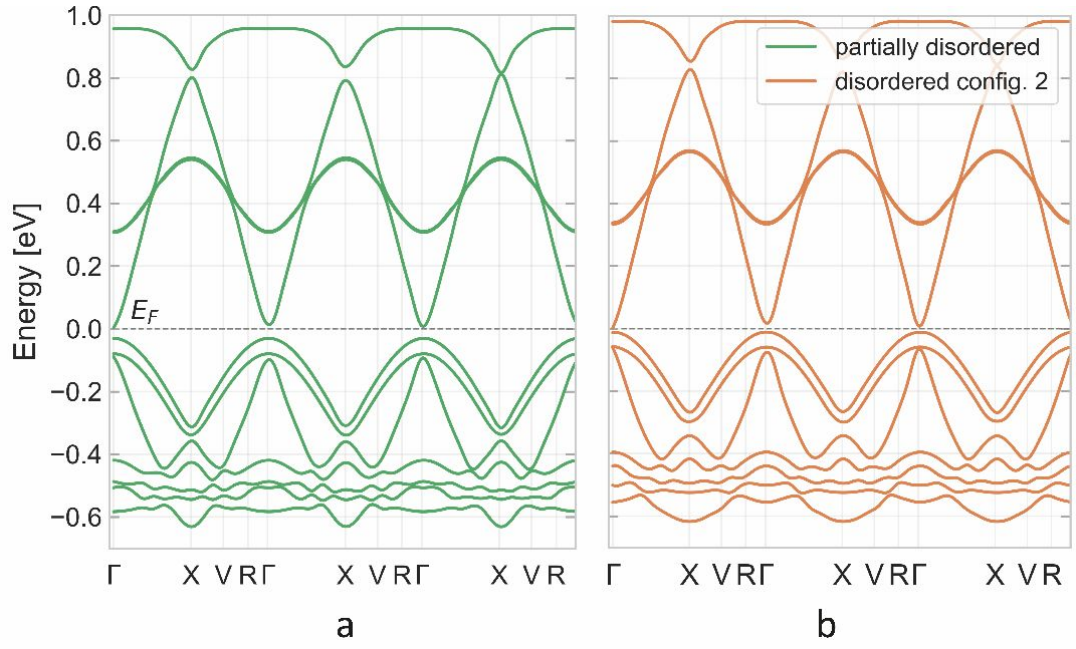

Figure S3. Band structures for partially disordered (a), and an additional configuration of fully disordered (b) kesterite. The Fermi energy is set to 0 eV in each case. X-axis is on the same scale in k-space.